

Article

Research on Statistical Characteristics and Prediction Methods of Ferronickel Slag Pervious Concrete Performance with Different Sizes of Aggregate and Mixtures

Zhongping Tang ^{1,2}, Hua Peng ², Shixiang Yi ¹ and Fan Feng ^{3,*} 

¹ Institute of Structural Material Failure and Strengthening Technology, Ningbo Polytechnic, Ningbo 315800, China; 2022005@nbpt.edu.cn (Z.T.); 1001554@nbpt.edu.cn (S.Y.)

² National Engineering Laboratory for Applied Technology of Forestry & Ecology in South China, Central South University of Forestry and Technology, Changsha 410075, China; 20220100066@csuft.edu.cn

³ School of Architectural Engineering, Hunan Institute of Engineering, Xiangtan 411100, China

* Correspondence: ff-fengfan@163.com

Abstract: In the exploration of sustainable construction materials, the application of ferronickel slag (FNS) in creating pervious concrete has been investigated, considering its potential to meet the dual requirements of mechanical strength and fluid permeability. To elucidate the statistical properties and models for predicting the performance of FNS-composited pervious concrete with different sizes of aggregates and mixtures, a series of experiments, including 54 kinds of mixtures and three kinds of aggregate, were conducted. The focus was on measuring the compressive strength and the permeability coefficient. The results indicate that the compressive strength of pervious concrete decreases with the increase in aggregate size, while the permeability coefficient increases with the increase in aggregate size. Through normalization, the variability of these properties was quantitatively analyzed, revealing coefficients of variation for the concrete's overall compressive strength and the permeability coefficient at 0.166, 0.132, and 0.150, respectively. Predictive models were developed using machine learning techniques, such as Linear Regression, Support Vector Machines, Regression Trees, and Gaussian Process Regression. These models demonstrated proficiency in forecasting the concrete's compressive strength and permeability coefficient.

Keywords: ferronickel slag; pervious concrete; compressive strength; permeability coefficient; aggregate; machine learning



Citation: Tang, Z.; Peng, H.; Yi, S.; Feng, F. Research on Statistical Characteristics and Prediction Methods of Ferronickel Slag Pervious Concrete Performance with Different Sizes of Aggregate and Mixtures. *Buildings* **2024**, *14*, 1255. <https://doi.org/10.3390/buildings14051255>

Academic Editor: Elena Ferretti

Received: 24 March 2024

Revised: 23 April 2024

Accepted: 27 April 2024

Published: 29 April 2024



Copyright: © 2024 by the authors. Licensee MDPI, Basel, Switzerland. This article is an open access article distributed under the terms and conditions of the Creative Commons Attribution (CC BY) license (<https://creativecommons.org/licenses/by/4.0/>).

1. Introduction

Pervious concrete, recognized for its high permeability, is commonly utilized in road-paving applications, where the balance between permeability and mechanical strength is crucial. This unique concrete blend primarily comprises coarse aggregates, water, and cementitious materials, deliberately omitting fine aggregates to enhance its porous structure and, consequently, its permeability.

Recent scholarly endeavors have explored various aspects of pervious concrete's performance. Huang et al. [1] delved into the resilience of innovative self-compacting recycled pervious concrete when subjected to the combined effects of freeze–thaw cycles and fatigue due to rainstorms. Meanwhile, Lee et al. [2] scrutinized the characteristics of pervious concrete, both of high strength and of conventional strength, when augmented with either steel or glass fibers, employing fifteen distinct mixes of these materials. Further, Lee et al. [3,4] broadened their research scope to examine the influence of advanced reinforcement materials, such as steel wire and glass fiber meshes, on the flexural strength of standard pervious concrete. They concentrated on key design variables, including the elastic modulus, modulus of rupture, and stress–strain behavior under various loading conditions. Gao et al. [5] conducted a study assessing the viability of using ceramsite as an aggregate in pervious

concrete, analyzing permeability across different aggregate types and water–cement ratios. Their findings underscored the advantages of ceramsite for enhancing the sustainability and longevity of infrastructure projects. In an investigation into the impact of aggregate size and compaction degree on pervious concrete, Ferić et al. [6] evaluated eleven different mix proportions by adjusting the aggregate fractions. Adil et al. [7] focused on the effect of silica fume on pervious concrete, observing that a 5% inclusion rate significantly improved the workability, strength, and durability of the concrete mix.

Pervious concrete's performance, encompassing aspects such as strength, permeability, and resistance to wear, diverges from that of traditional concrete due to the absence of fine aggregate. This distinction necessitates unique mix-design methods, as conventional approaches are unsuitable. The interplay between performance indicators often presents a challenge, prompting researchers to focus on developing mix proportioning and predictive models that harmonize these factors [8–11]. Yan et al. [12] explored the effects of adding granulated blast-furnace slag, hydroxypropyl methylcellulose, and polypropylene plastic textile fiber on the mechanical and permeability characteristics of pervious concrete. Through gray correlation analysis, the study optimized the mix, resulting in enhanced mechanical properties. Zhang et al. [13] validated the application of Response Surface Methodology for configuring the mix ratio of recycled aggregate pervious concrete, considering the internal structure's impact on strength and porosity, which includes the paste attributes, paste-coating thickness on aggregate surfaces, and the aggregate's void ratio.

The integration of innovative materials into concrete, along with the expanding variety of concrete components and the escalating demands for its performance, has introduced complexity into the prediction of concrete mix proportions and their performance outcomes. In light of these complexities, several researchers have advocated for the adoption of machine learning techniques to forecast performance and devise mix designs for concrete. For instance, Han et al. [14] utilized a random forest algorithm, a type of machine learning model, to estimate the compressive strength and dry density of concrete made with recycled plastic aggregates. This approach underscored the importance of precisely forecasting two fundamental attributes—the permeability coefficient and the uniaxial compressive strength—prior to the concrete's application in the field, aiming to curtail both the time and costs associated with construction projects. Given the challenge of modeling the intricate non-linear interactions between the permeability coefficient and its influencing factors using conventional mathematical models, Zhang et al. [15] tackled this issue by implementing a hybrid artificial intelligence model, specifically a multi-output least squares support vector regression. This innovative model further enhanced the accuracy of predictions by leveraging the interdependence between the permeability coefficient and uniaxial compressive strength.

Due to its excellent drainage capabilities, pervious concrete has become a preferred material in construction. Assessing its key characteristics, namely the permeability coefficient and the 28-day unconfined compressive strength, is essential before its utilization. However, the process of testing these properties, which is influenced by various factors, is both time-intensive and expensive. In response, Sun et al. [16] introduced an innovative approach by applying an advanced support vector regression model, which was fine-tuned using the beetle antennae search algorithm. This method was proposed to efficiently and accurately forecast the permeability coefficient and the uniaxial compressive strength of pervious concrete, marking a significant advancement in the field.

As a composite material, concrete faces variability in performance, production, and curing processes among its components, leading to uncertainty in its overall performance, including that of pervious concrete. The interactions between its components add to this uncertainty, impacting the quality and characteristics of the final concrete product. Therefore, some scholars have conducted research specifically on the uncertainty of concrete performances; for example, Jayasuriya et al. [17] collected experimental data from 115 published articles about hardened concrete properties made with recycled concrete aggregates and conducted statistical analysis. Hou et al. [18] studied a statistical model

for the compressive strength of cement materials and proposed a statistical model based on probability principles and fracture criteria, revealing the physical mechanism by which porous structures lead to a decrease in compressive strength. Ding et al. [19] collected 301 groups of experimental data on self-compacting steel fiber-reinforced concrete and conducted statistical analysis on its performance. Sonebi and Bassuoni [20] conducted a statistical modeling study on the mix design of pervious concrete, and the proposed statistical model can promote the optimization of PCPC mix proportions to achieve the target performance by reducing the required number of test batches.

Energy conservation, emission reduction, and solid waste management have become key issues for numerous countries globally. Using some solid waste to produce pervious concrete can effectively treat solid waste while reducing the use of construction materials and carbon emissions [21]. Many scholars have conducted research including using solid waste, such as recycled coarse aggregate [22–24], coal bottom ash aggregates [25], rice husk ash [26], waste glass [27], metakaolin [28], and fly ash [29], to produce pervious concrete.

Pentlandite, with its substantial mining output, generates a considerable amount of solid waste. The characteristics and particle size distribution of ferronickel slag (FNS) powder mirror those of various mineral admixtures used in concrete production. Accordingly, researchers have suggested the integration of FNS into concrete mixtures as a binder: for example, Bao et al. [30] used FNS as fine aggregate in the preparation of recycled concrete; Qi et al. [31] used FNS powder as a cementitious material to prepare concrete and conducted a study on its mechanical properties; You et al. [32] tried to prepare cementitious materials using alkali-excited FNS powder; Kim et al. [33] also used FNS powder as a cementing material to prepare concrete; and Saha and Sarker [34] used FNS as fine aggregate for the preparation of concrete and discussed its durability characteristics.

Many research results have shown that the size and shape of aggregates have a significant impact on the performance of concrete [35,36], and pervious concrete not only meets the performance requirements of ordinary concrete but also increases the demand for permeability. The selection of aggregates also has a certain impact on the dispersion of performance indicators of pervious concrete. This study aims to investigate the use of FNS as a cementitious material in the creation of pervious concrete, and the influences of aggregate particle size on the mechanics and water permeability of FNS pervious concrete were the focal points, and the statistical properties of its permeability coefficient and strength were also discussed. Additionally, in view of multiple parameters, such as aggregate size, mix ratio, and multiple targets, such as strength and permeability coefficients, traditional prediction models face difficulties in predicting multiple objectives, and currently, machine learning has gained many successful experiences in predicting concrete properties [37–39]; therefore, some machine learning techniques were employed to predict critical performance indices.

2. Materials, Mixtures, and Methods

2.1. Materials

The basic materials used include cement, FNS powder, pervious concrete reinforcement agents, water, and aggregates. The aggregate consists of three types, as shown in Figure 1. The first type (Aggregate C) was black gravel, also called Quartz conglomerate, with a size of 5–10 mm, and its edges were not sharp; the second type (Aggregate B) was also black gravel, with a size of 10–15 mm; the third type (Aggregate A) was Basalt stones, with a size of 10–20 mm and sharp edges.

The cement adopted a specification of P.O.42.5 Portland cement. The reinforcing agents for pervious concrete were provided by the Nanjing Hainiu Company. The ferronickel slag comes from the waste slag produced by a nickel–iron ore in Fuzhou, which has a large and uneven particle size and needs to be ground into powder, as shown in Figure 2. Figures 3 and 4 show the XRD patterns and surface spectrogram of FNS powder, and they demonstrate that the main components of FNS are CaO, SiO₂, Al₂O₃, and MgO, and the proportion of these were 35.58%, 30.91%, 16.71%, and 10.27%, respectively. These components provide a foundation for FNS to become a cementitious material.



Figure 1. Aggregates: (a) black gravel with size of 5–10 mm; (b) black gravel with size of 10–15 mm; (c) Basalt stones with size of 10–20 mm.

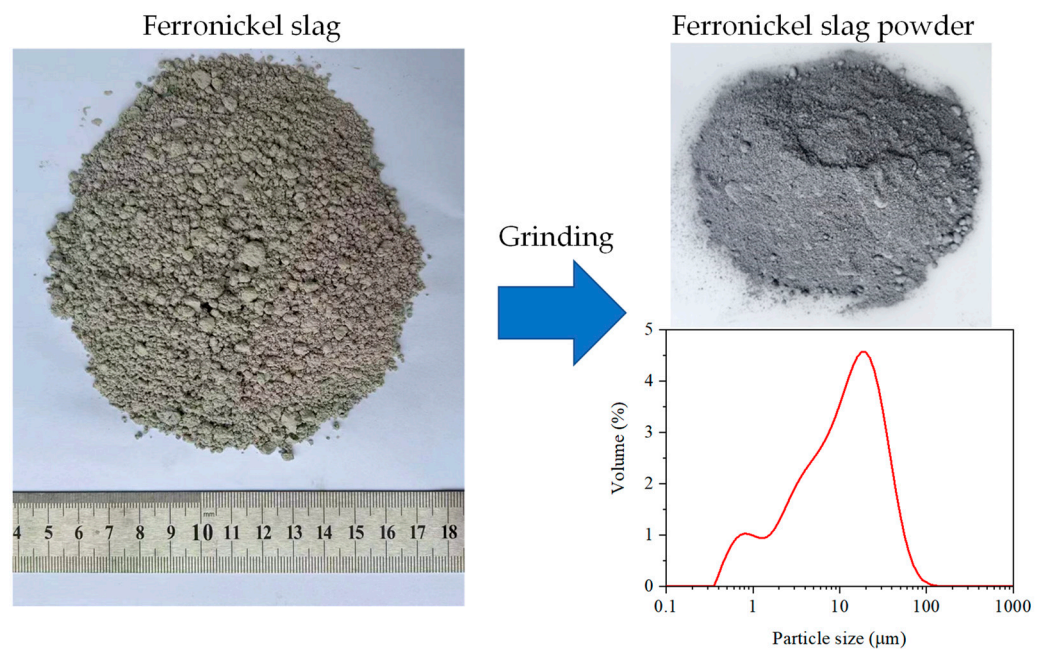


Figure 2. Nickel–iron ore waste residue and FNS powder.

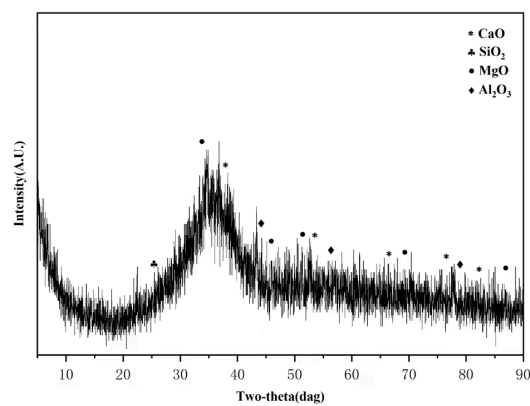


Figure 3. XRD patterns for FNS powder.

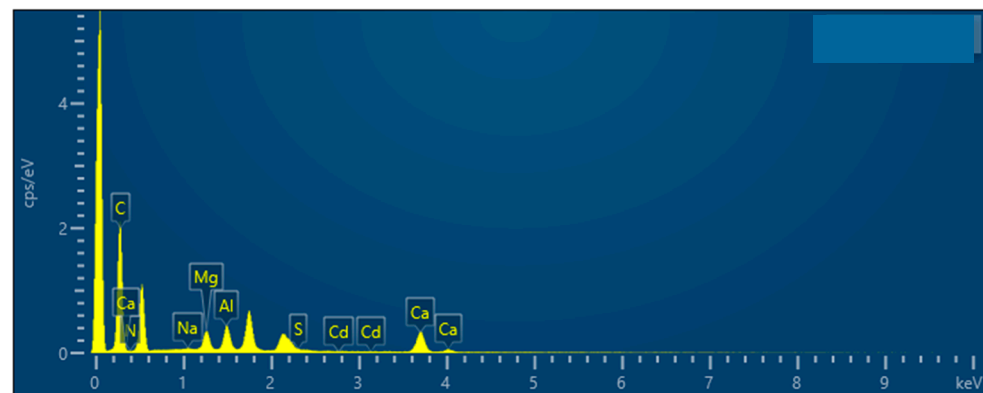


Figure 4. Total spectrum of chemical elements.

2.2. Mixtures

To evaluate the effect of aggregate size on the compressive strength and permeability coefficient of FOPC, a total of 54 mixtures were designed, as shown in Table 1, and six cubes with a size of 100 mm were prepared for each mixture. The ratio of water to cement (W/C) of each concrete test block was close, including 0.453, 0.45, and 0.44, so it could be considered that the same W/C was used. The concrete parameters included the type of aggregate, the ratio of cementitious material to Aggregate (C/A), and the substitution rate of FNS powder. The substitution rates of FNS varied across six levels: 0%, 10%, 20%, 30%, 40%, and 50%, respectively. The sample of the completed FOPC test block is shown in Figure 5.

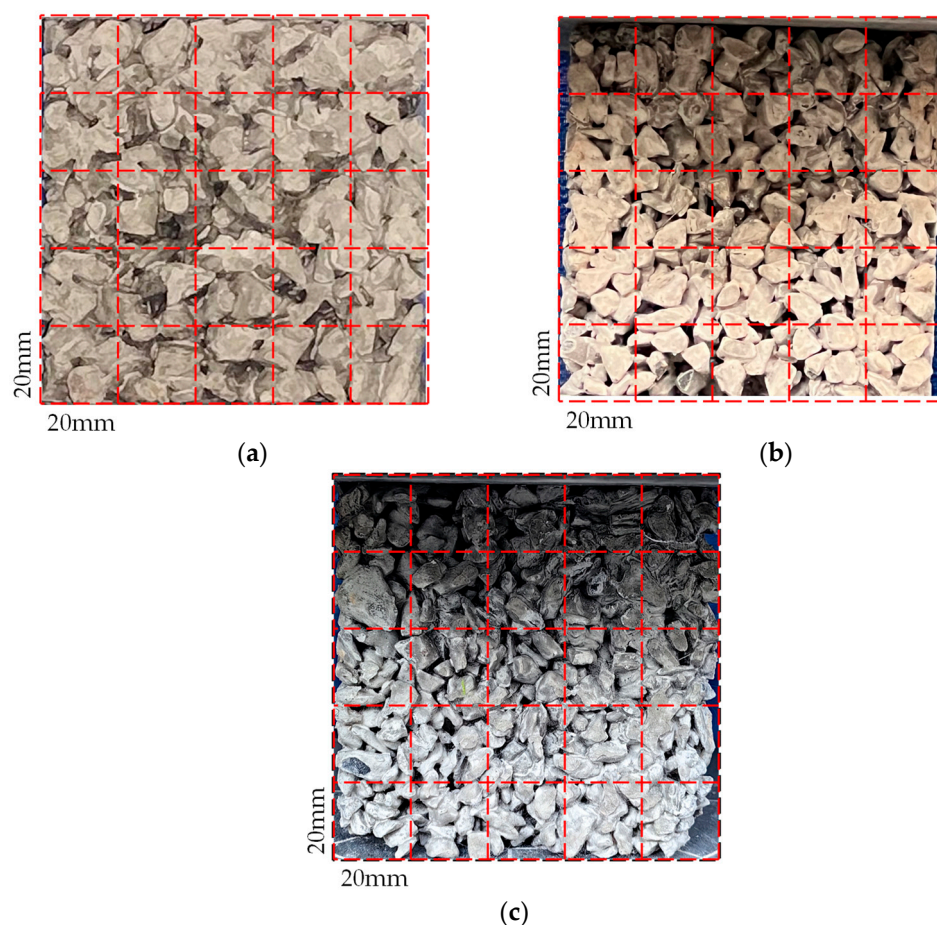


Figure 5. Cubes of FOPC: (a) FOPC-A; (b) FOPC-B; (c) FOPC-C.

Table 1. Mixtures of FOPC.

Group	Component Name	Coarse Aggregate (kg)	Cementitious Material (kg)		Reinforcing Agent (kg)	Water (kg)
			OPC	FNS		
FOPC-A	FOPC-A-1-0	1600	300	0	10	136
	FOPC-A-1-10	1600	270	30	10	136
	FOPC-A-1-20	1600	240	60	10	136
	FOPC-A-1-30	1600	210	90	10	136
	FOPC-A-1-40	1600	180	120	10	136
	FOPC-A-1-50	1600	150	150	10	136
	FOPC-A-2-0	1600	320	0	12	144
	FOPC-A-2-10	1600	288	32	12	144
	FOPC-A-2-20	1600	256	64	12	144
	FOPC-A-2-30	1600	224	96	12	144
	FOPC-A-2-40	1600	192	128	12	144
	FOPC-A-2-50	1600	160	160	12	144
	FOPC-A-3-0	1600	350	0	15	154
	FOPC-A-3-10	1600	315	35	15	154
	FOPC-A-3-20	1600	280	70	15	154
FOPC-B	FOPC-B-1-0	1600	300	0	10	136
	FOPC-B-1-10	1600	270	30	10	136
	FOPC-B-1-20	1600	240	60	10	136
	FOPC-B-1-30	1600	210	90	10	136
	FOPC-B-1-40	1600	180	120	10	136
	FOPC-B-1-50	1600	150	150	10	136
	FOPC-B-2-0	1600	320	0	12	144
	FOPC-B-2-10	1600	288	32	12	144
	FOPC-B-2-20	1600	256	64	12	144
	FOPC-B-2-30	1600	224	96	12	144
	FOPC-B-2-40	1600	192	128	12	144
	FOPC-B-2-50	1600	160	160	12	144
	FOPC-B-3-0	1600	350	0	15	154
	FOPC-B-3-10	1600	315	35	15	154
	FOPC-B-3-20	1600	280	70	15	154
FOPC-C	FOPC-C-1-0	1600	300	0	10	136
	FOPC-C-1-10	1600	270	30	10	136
	FOPC-C-1-20	1600	240	60	10	136
	FOPC-C-1-30	1600	210	90	10	136
	FOPC-C-1-40	1600	180	120	10	136
	FOPC-C-1-50	1600	150	150	10	136
	FOPC-C-2-0	1600	320	0	12	144
	FOPC-C-2-10	1600	288	32	12	144
	FOPC-C-2-20	1600	256	64	12	144
	FOPC-C-2-30	1600	224	96	12	144
	FOPC-C-2-40	1600	192	128	12	144
	FOPC-C-2-50	1600	160	160	12	144
	FOPC-C-3-0	1600	350	0	15	154
	FOPC-C-3-10	1600	315	35	15	154
	FOPC-C-3-20	1600	280	70	15	154
	FOPC-C-3-30	1600	245	105	15	154
	FOPC-C-3-40	1600	210	140	15	154
	FOPC-C-3-50	1600	175	175	15	154

Note: FOPC-A denotes FOPC with black gravel with size of 5–10 mm; FOPC-B denotes FOPC with black gravel with size of 10–15 mm; FOPC-C denotes FOPC with Basalt stones with size of 10–20 mm.

To ensure the controllability of sample quality, all samples were prepared within a week, and the weather and temperature were similar on each day of preparation. Except for the aggregate, all cement and FNS powders were produced by the same company, respectively. The concrete mixing time was three minutes for all concrete samples.

2.3. Test Method

2.3.1. Compressive Strength

Concrete's strength encompasses various types, such as compressive, tensile, flexural, and shear strengths. Predominantly utilized for road paving, pervious concrete is primarily subjected to compressive forces. Hence, the focus is usually on assessing its compressive strength. As per the standard GB/T50081-2016 [40], the evaluation of concrete specimens involves measuring their compressive strength and noting the peak load at the point of failure. The formula to calculate the compressive strength f_c of concrete is given by the following:

$$f_c = 0.95 \frac{F}{A} \quad (1)$$

In this equation, F represents the maximum load sustained at failure, while A denotes the area subjected to compression. Before loading, the dimension of the component was measured to ensure that the error was within 3 mm to ensure the reliability of the measured results.

2.3.2. Porosity

Every block underwent porosity testing, which was conducted in accordance with the pertinent procedures outlined in the CJJ/T135-2009 standard [41], and the porosity p could be calculated using the following formula:

$$p = 1 - \frac{m_2 - m_1}{\rho_w V_0}, \quad (2)$$

where ρ_w denotes the density of water; m_1 denotes the mass of the dried test specimen, and each test specimen was placed in a drying oven at 60 degrees Celsius for 24 h to ensure the accuracy of the test; m_2 denotes the mass of the test specimen in water; and V_0 denotes the volume of the block.

2.3.3. Permeability Coefficient

The permeability performance of pervious concrete was quantified using the permeability coefficient, which can be measured through two primary methods: the constant head and the variable head methods [42]. The constant head method is optimal for high permeability materials like sand and gravel, while the variable head method is better suited for materials with finer particles, such as fine-grained soils. Given the nature of pervious concrete discussed in this study, the constant head method emerged as the more fitting choice. Although the standard CJJ/T135-2009 [41] outlines a procedure for measuring the pavement permeability coefficient on-site, which primarily employs the variable head method for its practicality in field applications and to safeguard pervious pavements, this research opted for the constant head method. This decision was based on prior experiences and the suitability of the two methods for different materials, as demonstrated in Figure 6.

To ascertain the permeability coefficient using this apparatus, the procedure begins by accurately positioning the prepared pervious concrete specimen within the device's sleeve. The interface between the block and sleeve is then sealed with a molding agent to prevent water from bypassing the concrete through gaps. Upon initiating the test, water is introduced at the inlet, filling the system. To maintain a constant water level difference, water is allowed to exit through both the upper and lower drainage outlets simultaneously. Once a stable water level difference is established, the stopwatch is started, and water addition continues. The water exiting from the lower outlet is collected, and the volume Q

is measured over time t . The permeability coefficient for the specimen is calculated using Darcy's law, expressed as follows:

$$k = \frac{QL}{Aht} \quad (3)$$

Here, Q represents the volume of water collected (m^3), L is the thickness of the concrete block (m), A is the cross-sectional area of the block (m^2), and h is the water head difference (m).

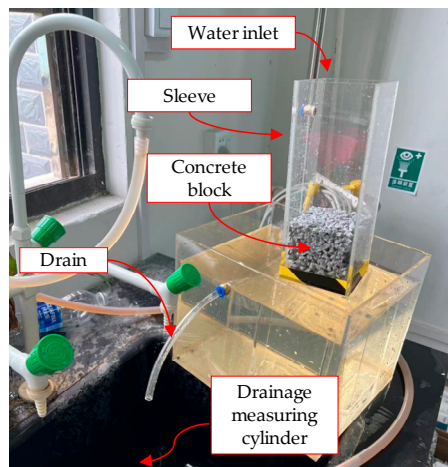


Figure 6. Permeability coefficient testing device.

3. Test Results

3.1. Compressive Strength

The average compressive strength of pervious concrete under different parameters is shown in Figure 7. For the case of $C/A = 0.1875$ (Figure 7a), it could be seen that when the FNS substitution rate was the same, the FOPC-A group had the smallest strength, followed by the FOPC-B group, and the FOPC-C group has the largest strength. Compared with the FOPC-A group, the strengths of the FOPC-B group and FOPC-C group increased by 7.4–13% and 14–24%, respectively; similarly, in the case of $C/A = 0.2000$ (Figure 7b), when the FNS substitution rate was the same, the FOPC-A group had the lowest strength, followed by FOPC-B group, and FOPC-C group had the highest strength. Compared with the FOPC-A group, the strengths of the FOPC-B group and the FOPC-C group increased by 3–6% and 7–15%, respectively; in the case of $C/A = 0.2188$ (Figure 7c), compared with the FOPC-A group, the strengths of the FOPC-B group and the FOPC-C group increased by 5–8% and 5–16%, respectively.

Overall, from an average perspective, the size of the aggregates has an impact on the strength of pervious concrete, and the strength decreases with the increase in aggregate size. However, there were also some exceptions; for example, when C/A was 0.1875 and the FNS substitution rate was 30%, the concrete strength using Aggregate B was very close to that using Aggregate C; when C/A was 0.2000 and the FNS substitution rates were 30%, 40%, and 50%, the concrete strength using Aggregate B was very close to that using Aggregate C; when C/A was 0.2188 and the FNS substitution rate was 40%, the concrete strength using Aggregate B was greater than that using Aggregate C. This is because the water–cement ratio is small, and due to the absence of fine aggregates, the flowability of pervious concrete is poor. The larger the size of the aggregates, the worse their flowability, resulting in a larger porosity during the production of concrete specimens, which further leads to a decrease in the strength of the concrete; this is consistent with the conclusion of the literature [6].

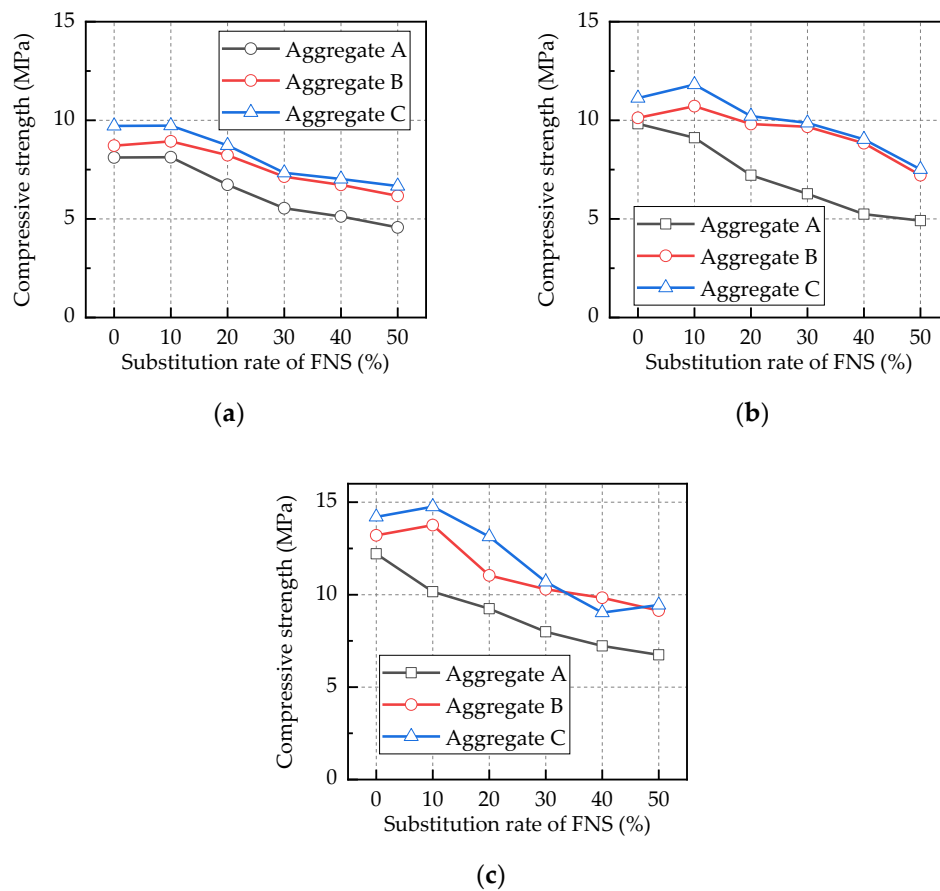


Figure 7. Compression strength of FOPC: (a) $C/A = 0.1875$; (b) $C/A = 0.2000$; (c) $C/A = 0.2188$.

In addition, the compressive strength of concrete decreases with the increase in the FNS substitution rate. The comparison between the FNS substitution rate and the decrease rate of concrete compressive strength is shown in Figure 8. For pervious concrete using Aggregate A, the strength reduction rate was relatively high. Except for the case where the substitution rate was 10%, most of the strength reduction rates exceeded the substitution rate, indicating that FNS did not play a significant role; for pervious concrete using Aggregate B, the strength reduction rate was small, and all concrete strength reduction rates were lower than the substitution rate. Most of the strength reduction rates were 10–25% lower than the FNS substitution rate, with a maximum difference of 27%; for pervious concrete using Aggregate C, all concrete strength reduction rates were lower than the substitution rate, with most strength reduction rates being 8–26% lower than the FNS substitution rate, with a maximum difference of 29%. These results indicate that the strength contribution of FNS in pervious concrete using Aggregate B and Aggregate C was significant, and this indicates that FNS plays a role as a cementitious material to a certain extent, and it is more pronounced at low substitution rates. This is because the alkaline substances in cement stimulate the activity of substances in FNS, like CaO , SiO_2 , Al_2O_3 , and MgO , making it have a cementitious effect.

In the work of Qi et al. [31], the strength of concrete decreased by 3.69%, 2.39%, 2.39%, 10.85%, and 19.09% when the FNS content was 10%, 20%, 30%, 40%, and 50%. In the case of small substitution rates (below 30%), the strength reduction of FOPC was similar to that of the research results, while in the case of large substitution rates (above 30%), the strength reduction of FOPC was greater than that of the research results. Overall, however, the pattern was consistent with the pattern found in this paper.

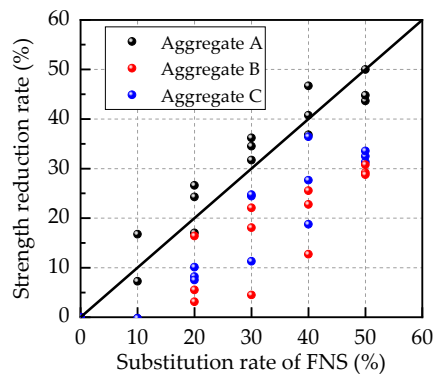


Figure 8. The reduction rate of compressive strength of pervious concrete.

However, the coagulation effect of FNS was not significant in the FOPC-A group; this is mainly due to the incomplete hydration reaction of pervious concrete using Aggregate A during mixing and specimen production. Of course, this can also be seen in the process of making test blocks, as various parts cannot be quickly and effectively mixed together. This also makes it difficult for alkaline substances in cement to activate the substances in FNS. However, pervious concrete using Aggregate B and Aggregate C had better flowability and sufficient hydration reaction. This finding is consistent with the results of Huang et al. [43], in which the influence of different aggregate particle sizes on the strength of recycled concrete was compared. The aggregate particle sizes were 5–10 mm, 10–16 mm, and 20–25 mm, respectively. Under different aggregate substitution rates, the strength decreased with the increase in aggregate particle size.

3.2. Porosity

By cutting the test blocks of three different aggregates with $C/A = 0.2000$, as shown in Figure 9, it could be seen that the pores of the FOPC-A group and the FOPC-C were distributed uniformly, and they were abundant and small, while the pores of the FOPC-B group were more concentrated and larger.

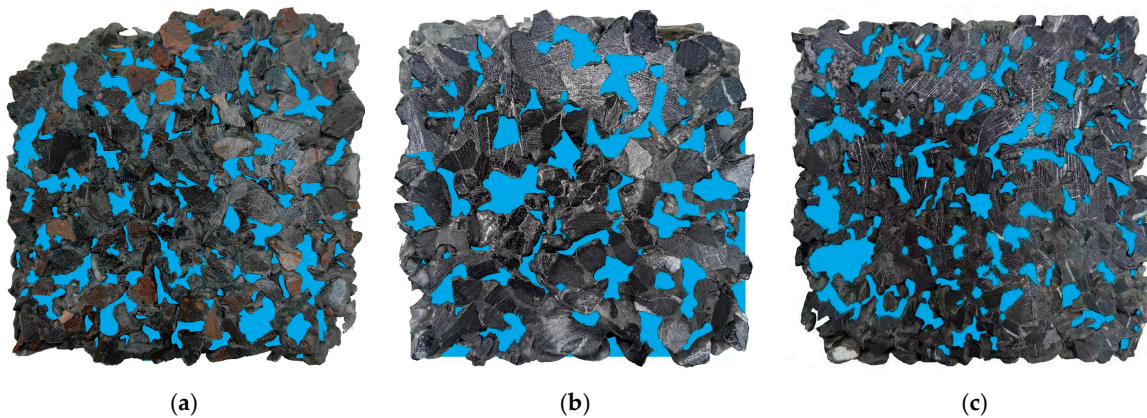


Figure 9. Test block after cutting: (a) FOPC-A; (b) FOPC-B; (c) FOPC-C.

The average porosity of pervious concrete with different parameters is shown in Figure 10. It could be seen that the influence of FNS content on porosity followed no obvious rule, but the selected aggregate had an impact on porosity. Among them, the porosity corresponding to the FOPC-A group was the largest, followed by that of the FOPC-B group, and that of the FOPC-C group was the smallest. In other words, under the same mixture, the porosity increases with the increase in aggregate particle size. This is because concrete with a large aggregate size has small fluidity, and it is easy to have a hole in the middle during the process of mixing and making test blocks, while concrete with a

small aggregate size can be made denser inside by vibrating during the process of mixing and making test blocks.

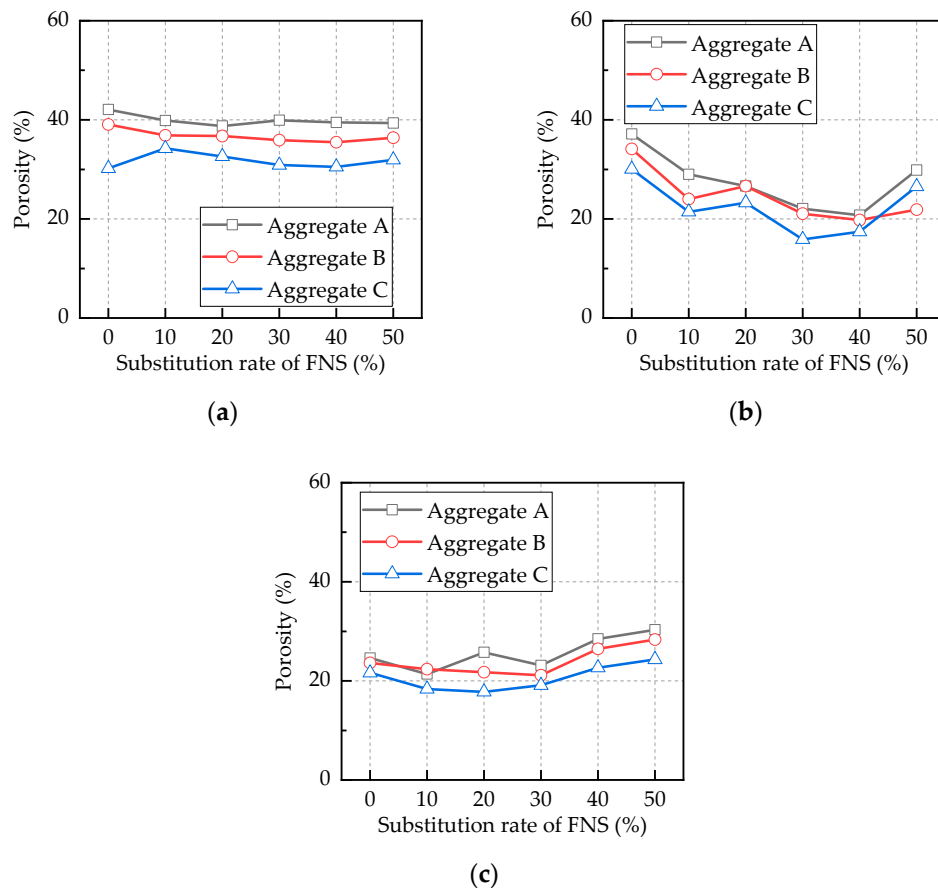


Figure 10. Porosity: (a) $C/A = 0.1875$; (b) $C/A = 0.2000$; (c) $C/A = 0.2188$.

3.3. Permeability Coefficient

The average permeability coefficient of pervious concrete with different parameters is shown in Figure 11. It could be seen that the effect of FNS content on the permeability coefficient was not obvious, but the selected aggregate had an effect on the permeability coefficient. For the case of $C/A = 0.1875$ (Figure 11a), it could be seen that when the FNS substitution rate was the same, the permeability coefficient of the FOPC-A group was the largest, followed by the strength of the FOPC-B group, and the permeability coefficient of the FOPC-C group was the smallest. Compared with the FOPC-A group, the permeability coefficients of the FOPC-B group and the FOPC-C group were reduced by 4–15% and 13–23%, respectively. For the case where $C/A = 0.2000$ (Figure 11b), similarly, when the FNS substitution rate was the same, the permeability coefficient of the FOPC-A was the largest, followed by the strength of the FOPC-B group, and the permeability coefficient of the FOPC-C group was the smallest. Compared with the FOPC-A group, the permeability coefficients of the FOPC-B group and the FOPC-C group were reduced by 4–9% and 14–18%, respectively. For the case where $C/A = 0.2188$ (Figure 11c), compared with the FOPC-A group, the permeability coefficients of the FOPC-B group and the FOPC-C group were reduced by 2–4% and 8–22%, respectively. This is because the porosity of concrete with a large aggregate size is large, and the porosity directly affects the permeability coefficient.

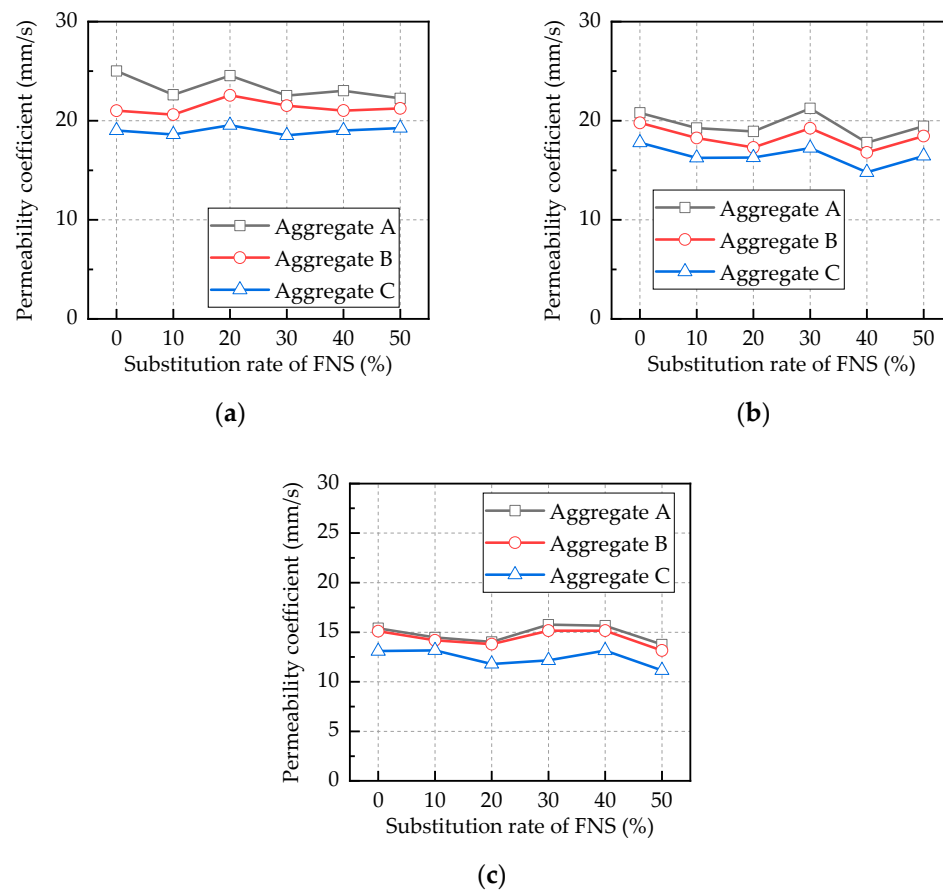


Figure 11. Permeability coefficient: (a) $C/A = 0.1875$; (b) $C/A = 0.2000$; (c) $C/A = 0.2188$.

3.4. Indicator Discussion

Many literature results indicate that the porosity of pervious concrete has a significant impact on the permeability coefficient [44–46]. This is because the permeability function of pervious concrete is mainly due to the presence of many pores in the concrete, allowing water to flow through the pores and pass through the concrete. In addition, porosity also has a significant impact on the compressive strength of concrete.

The comparison between the average porosity and average compressive strength of the test block is shown in Figure 12. It can be seen that overall, the compressive strength decreases with the increase in porosity.

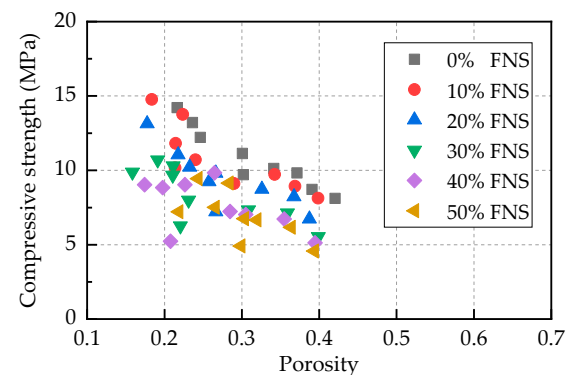


Figure 12. Porosity vs. compressive strength.

The comparison between the average porosity and average permeability coefficient of the test block is shown in Figure 13. It can be seen that overall, the average permeability coefficient increases with the increase in porosity.

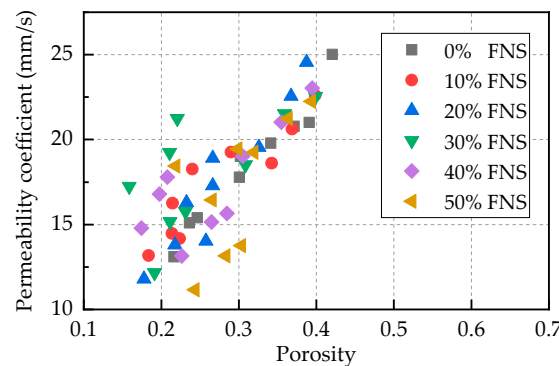


Figure 13. Porosity vs. permeability coefficient.

4. Statistical Analysis

4.1. Compressive Strength

The compressive strength of pervious concrete is significantly influenced by the ratio of C/A, the water-to-cement ratio (W/C), and the size of the aggregate. Variability in porosity and distribution of aggregate introduces uncertainties during the mixing process. Figure 14 illustrates the statistical analysis of compressive strength test results for pervious concrete with varying mix proportions and aggregates.

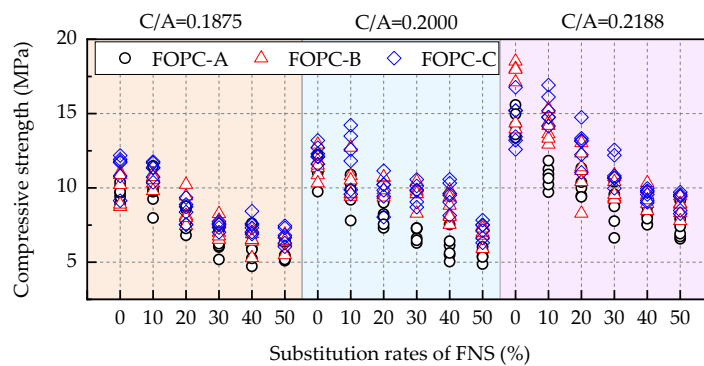


Figure 14. Compressive strength of FOPC with different samples.

Overall, the strength of concrete with different C/A decreased with the increase in the FNS substitution rate; the strength of concrete with different aggregates exhibited discreteness, and the degree of discreteness of concrete strength with different aggregates was similar. Under the same FNS substitution rate, the strength of concrete increased with the increase in C/A. However, due to the existence of discreteness, the strength of some concrete with a high C/A value was lower than that of concrete with a low C/A value.

To gain a clearer understanding of the statistical attributes of concrete's compressive strength, especially considering the minor variations in strength across different mix ratios, a normalized analysis was applied. This process was defined by the following equation:

$$f_{c,N} = \frac{f_{c,test}}{f_{c,\mu}} \quad (4)$$

Here, $f_{c,N}$ denotes the normalized strength of the concrete, $f_{c,test}$ represents the compressive strength obtained from testing, and $f_{c,\mu}$ is the average compressive strength of the concrete for a given mix ratio.

Figure 15 presents a normalized statistical histogram for the strength of the FOPC. It can be seen that the distribution of concrete strength with different aggregates roughly followed a normal distribution with a mean value of 1.0, and its range was from 0.7 to 1.3; comparing the distribution of different aggregates, the standard deviations of the FOPC-A group, the FOPC-B group, and the FOPC-C group were approximately 0.15, 0.13, and 0.10, respectively. Similarly, the coefficients of variation (COVs) were approximately 0.15, 0.13, and 0.10, respectively. The overall COV was approximately 0.132, and this COV aligns with that observed in other types of concrete [47].

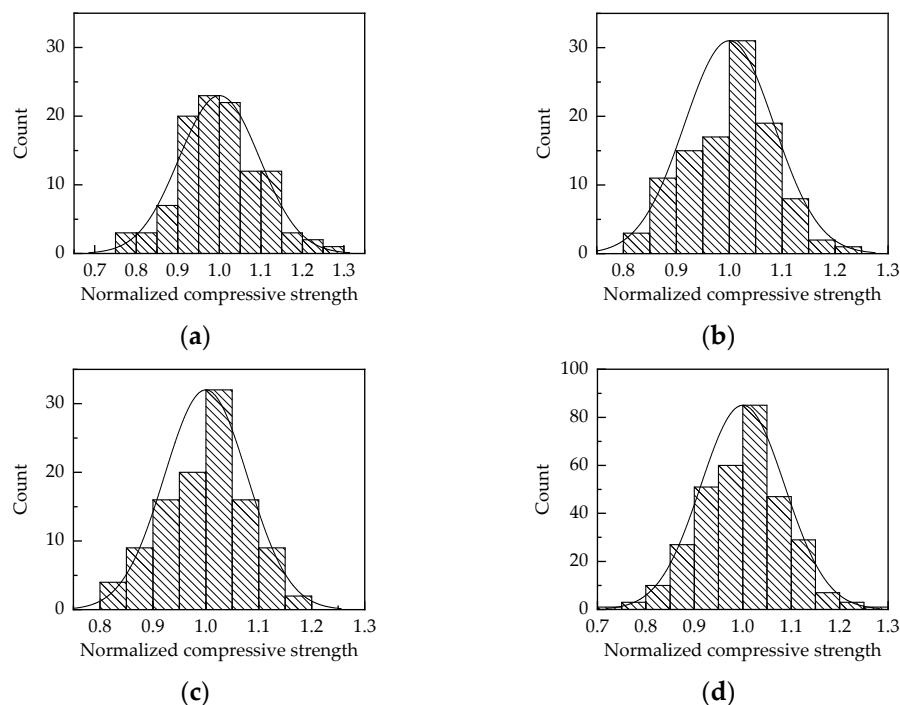


Figure 15. Statistics of normalized compressive strength: (a) FOPC-A group; (b) FOPC-B group; (c) FOPC-C group; (d) All samples.

4.2. Permeability Coefficient

The compressive strength of pervious concrete is significantly influenced by its porosity, which primarily depends on the C/A. During the mixing process, the random distribution of aggregates contributes to the variability in porosity. This will inevitably cause variability in the permeability coefficient. Figure 16 illustrates the statistical analysis of the permeability coefficient for pervious concrete with varying mix ratios and aggregates. It could be seen that the permeability coefficient decreased with the increase in C/A value, and there was little correlation with the content of FNS. Overall, the permeability coefficient of the FOPC-A group was the highest, followed by the FOPC-B group, and the FOPC-C group was the smallest. However, due to the existence of discreteness, some samples violated the above rules.

Similarly, to refine the analysis of the permeability coefficient's statistical properties in pervious concrete, a normalization approach was employed, defined as follows:

$$k_N = \frac{k_{N,test}}{k_{N,\mu}} \quad (5)$$

In this formula, k_N represents the normalized permeability coefficient, $k_{N,test}$ is the permeability coefficient measured in the test, and $k_{N,\mu}$ is the average permeability coefficient for a given mix ratio.

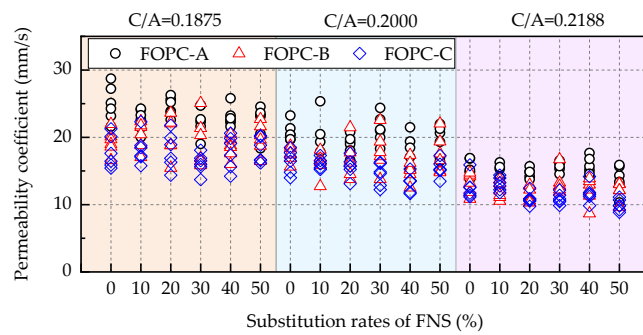


Figure 16. Permeability coefficient of FOPC with different samples.

Figure 17 presents a normalized statistical histogram for the permeability coefficient of FOPC. Compared with the strength of concrete, the dispersion of the permeability coefficient was greater, and the value of the normalized permeability coefficient of the FOPC-A group ranged from 0.7 to 1.30, which basically conformed to a normal distribution shape with a COV of about 0.15; the FOPC-B group ranged from 0.6 to 1.4, with a significant difference in morphology and normal distribution, with a COV of approximately 0.20; the FOPC-C group ranged from 0.7 to 1.3, with a significant difference in morphology and normal distribution, with a coefficient of variation of approximately 0.14; the overall COV was approximately 0.15.

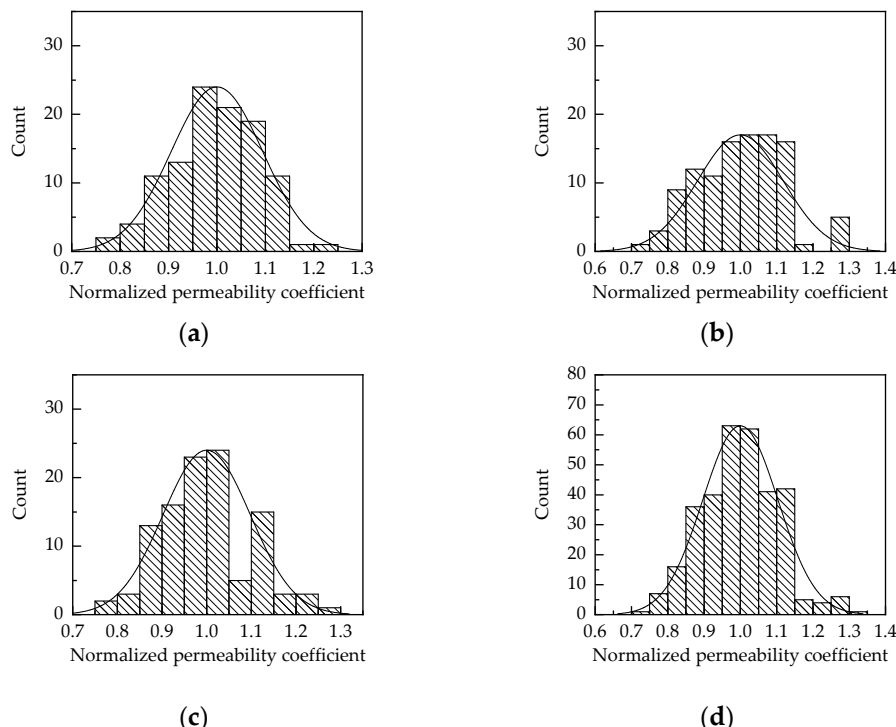


Figure 17. Statistics of normalized permeability coefficient: (a) FOPC-A group; (b) FOPC-B group; (c) FOPC-C group; (d) All samples.

5. Performance Predictions

5.1. Machine Learning Approaches

Section 4 highlighted the inherent variability in the strength and permeability coefficient of pervious concrete, notably in the permeability coefficient. This variability persists even when identical mix proportions are used, leading to differing outcomes. Consequently, this variance complicates the prediction of pervious concrete's performance. In response, the application of machine learning techniques has been suggested to analyze the test

results of pervious concrete and develop a predictive model. To achieve this, four machine learning methods were employed: Linear Regression (LR), Regression Trees (RTs), Support Vector Machines (SVMs), and Gaussian Process Regression (GPR), as illustrated in Figure 18.

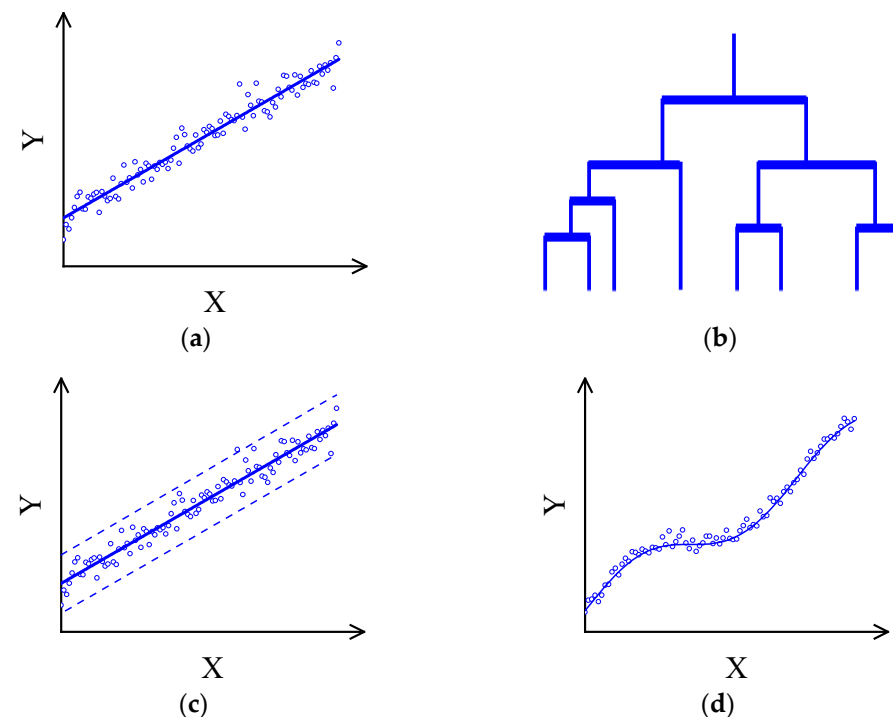


Figure 18. Schematic diagram of machine learning algorithms: (a) LR; (b) RT; (c) SVM; (d) GPR.

The Linear Regression (LR) algorithm constructs a model by identifying the optimal straight line that correlates data points [48]. This is represented by the equation $Y = mX + c$, where Y is the outcome variable and X represents the predictor variable. The coefficients m and c are determined based on the dataset. Linear Regression is categorized into Simple Linear Regression, which involves a single predictor variable, and Multiple Regression, which incorporates multiple predictors.

RTs and their variations operate by segmenting the input space into distinct regions, each defined by its own set of parameters [49]. By utilizing the structure of a tree, the journey from the root node to a leaf node embodies a set of rules leading to a classification, with each leaf node denoting a distinct output category. The process begins by dividing the data into several subsets, followed by further segmentation and recursion until each subset is homogenous. By starting at the root node, the algorithm tests each branch, progressing to the leaf nodes to determine the predicted category. This method is characterized by its straightforward structure and efficiency in handling data.

SVMs stand out in the realm of statistical learning for their unique approach, which diverges from conventional methodologies [50]. By simplifying the problem through space transformation and dimensionality increase, SVM transforms it into a classically solvable linear separation issue. Initially, it requires a shift to a higher-dimensional space through a non-linear transformation. Subsequently, an optimal linear classification plane is identified within this newly complexified space. The resultant classification function bears resemblance to that of neural network algorithms in structure.

GPR is a non-parametric approach that leverages Gaussian Processes prior to conducting regression analyses on datasets [51]. It adopts Gaussian Processes as the prior based on the premise that the observed dataset represents samples from Gaussian processes, making the estimation outcomes highly dependent on the choice of kernel function. The kernel function in GPR effectively acts as the covariance function, detailing the correlation

between the data points. Thus, it is integral to the model's foundational assumptions rather than merely serving as a computational shortcut via kernel methods. This section briefly introduces prevalent kernel functions used in GPR and discusses a method to expedite the computation of kernel functions.

5.2. Evaluation Method

To assess the precision of machine learning models, three metrics were utilized: RMSE, MAE, and MAPE.

5.2.1. RMSE

RMSE can be expressed as follows:

$$RMSE = \sqrt{\frac{1}{N} \sum_{i=1}^N (Y_p - Y_t)^2}, \quad (6)$$

where Y_p is the predicted response, Y_t is the test response, and N is the number of samples. The larger the RMSE, the greater the predicted error.

5.2.2. R^2

R^2 , also known as the coefficient of determination, is an indicator used to evaluate a model. It represents the proportion of the model's interpretable variance to the total variance, which can be expressed as follows:

$$R^2 = 1 - \frac{\sum_i (Y_p - \bar{Y})^2}{\sum_i (Y_t - \bar{Y})^2} \quad (7)$$

$R^2 = 1$ is the most ideal scenario, where all predicted values are equal to the true value. That is to say, the closer R^2 is to 1, the more accurate the predicted values are.

5.2.3. MAE

MAE calculates the average magnitude of errors in a set of predictions without considering their direction. It is determined by taking the absolute difference between each measurement and the overall average of these measurements. The formula for MAE is given by the following:

$$MAE = \frac{1}{N} \sum_{i=1}^N |Y_p - Y_t| \quad (8)$$

5.2.4. MAPE

MAPE serves as an assessment technique that addresses the shortcomings associated with the size-dependent errors found in MAE. It is characterized as follows:

$$MAPE(\%) = \frac{1}{N} \sum_{i=1}^N \left| \frac{Y_p - Y_t}{Y_t} \right| \times 100 \quad (9)$$

5.3. Prediction Based on Machine Learning

5.3.1. Compressive Strength

Figure 19 illustrates the comparison between the actual and predicted compressive strength of concrete, as determined by various machine learning methods. The horizontal axis denotes the actual values, while the vertical axis denotes the predicted ones. A closer alignment of the data points to the diagonal line indicates higher prediction accuracy. As depicted, most data points cluster near the diagonal, suggesting accurate predictions. The performance metrics for these predictions are summarized in Table 2. The coefficient of determination (R^2) highlights GPR's superior predictive capability, achieving 0.85, with

RT as the next best. GPR also leads in terms of RMSE, recording a score of 0.92, again followed by RT. For MAE, GPR showed the highest accuracy with a score of 0.72, with RT closely behind. Meanwhile, RT outperformed others in MAPE, registering 7.48%, with SVM following. On the whole, GPR demonstrated the most effective predictive accuracy.

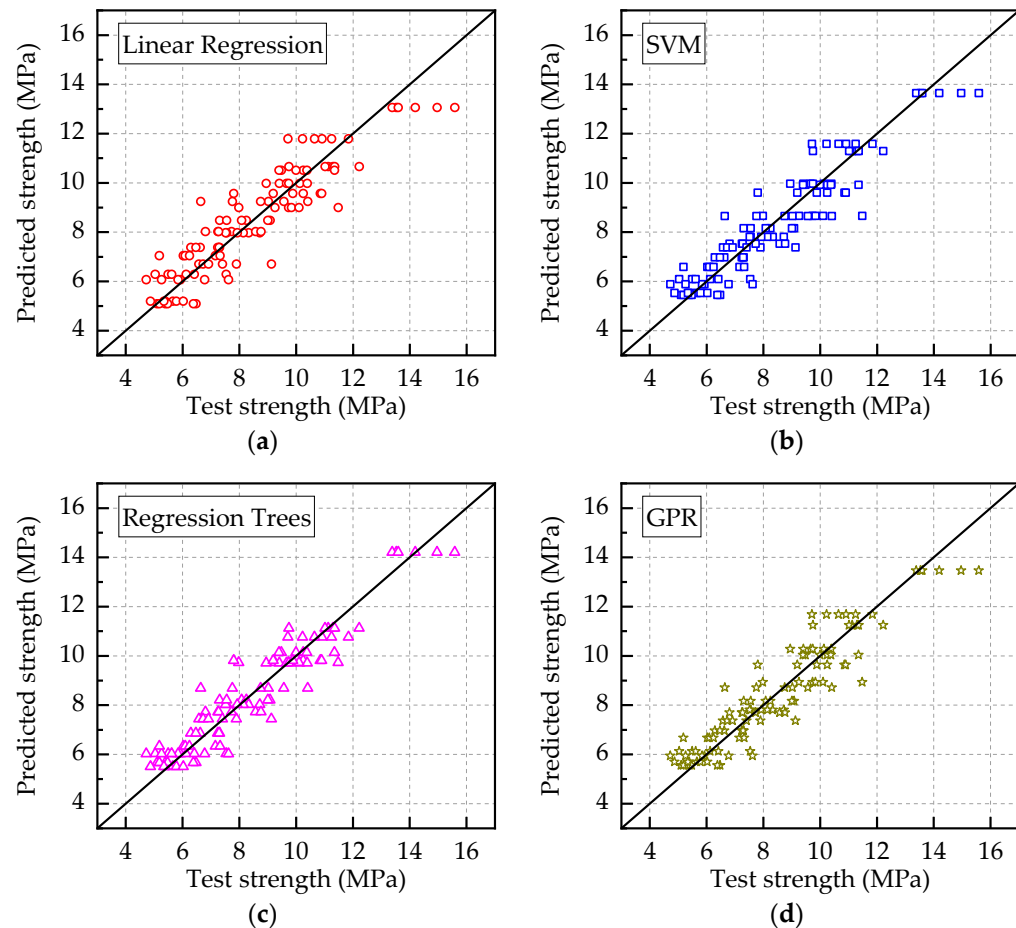


Figure 19. Prediction for concrete strength: (a) LR; (b) SVM; (c) RT; (d) GPR.

Table 2. Performance measures of compressive strength predicted model.

Approach	Performance Measures			
	R ²	RMSE (MPa)	MAE (MPa)	MAPE (%)
LR	0.83	0.97	0.79	9.13
SVM	0.81	1.04	0.81	8.17
RT	0.85	0.93	0.73	7.48
GPR	0.85	0.92	0.72	8.15

5.3.2. Permeability Coefficient

The machine learning predicting methods have demonstrated high precision in estimating the strength of concrete. Li et al. [44] highlighted a notable link between the permeability coefficient and porosity, with the latter being relatively straightforward to measure. Consequently, porosity has also been incorporated as a variable in the models.

Figure 20 depicts the comparison of the permeability coefficient values for concrete, as predicted by the refined models from various machine learning methods against actual measurements. The x-axis shows the actual values, while the y-axis displays the predicted values. Data points that align closely with the diagonal line indicate higher accuracy in the predictions.

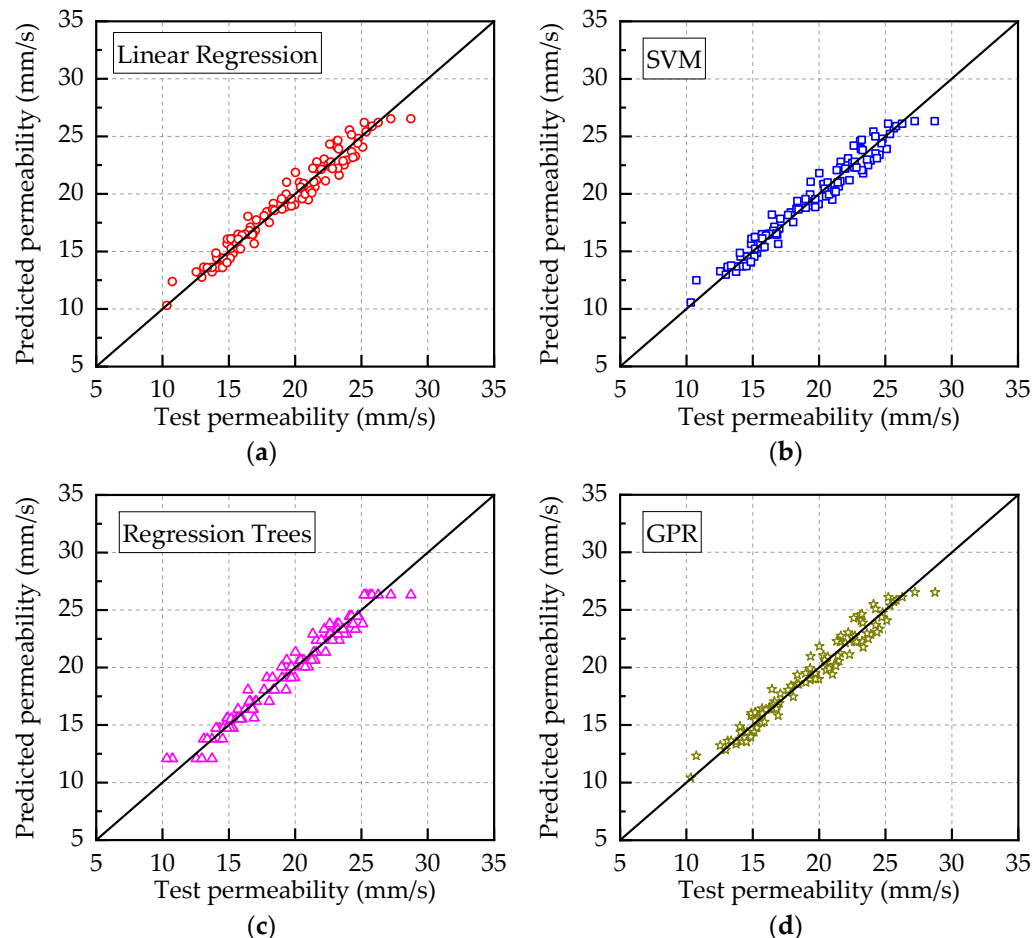


Figure 20. Updated model for predicting permeability coefficient: (a) LR; (b) SVM; (c) RT; (d) GPR.

Table 3 details the performance metrics for the model's prediction outcomes. LR showcased the most substantial improvement in R^2 , achieving 0.96; SVM led in RMSE with a score of 0.85, a marked decrease from the earlier 2.07; SVM again excelled in MAE, recording a low of 0.69, substantially down from the prior 1.59; RT demonstrated its strength in MAPE at 3.19%, significantly less than the former 7.43%. Overall, the revised model exhibits a marked increase in prediction accuracy, with SVM standing out as the top performer.

Table 3. Performance measures of permeability predicted model.

Approach	Performance Measures			
	R^2	RMSE (mm/s)	MAE (mm/s)	MAPE
LR	0.96	0.86	0.69	3.40
SVM	0.96	0.85	0.69	3.42
RT	0.94	1.01	0.82	3.19
GPR	0.95	0.88	0.70	3.38

6. Conclusions

To elucidate the statistical behavior of the compressive strength and permeability coefficient of FOPC with different sizes of aggregate and mixtures, alongside understanding its performance index forecasting, a series of performance evaluations were conducted. These evaluations included testing the compressive strength and permeability coefficients of FOPC. The analysis of these indices revealed their statistical properties, and machine

learning techniques were applied for performance prediction. The findings are summarized as follows:

(1) Overall, the compressive strength of FOPC decreases with the increase in aggregate size, increases with the increase in C/A, and decreases with the increase in FNS substitution rate. However, due to the existence of discreteness, some samples do not follow these rules.

(2) The permeability coefficient of FOPC increases with the increase in aggregate size and decreases with the increase in C/A, while this is not closely related to the FNS substitution.

(3) The porosity of FOPC has a significant impact on its strength and permeability coefficient. Specifically, as the porosity increases, the strength decreases while the permeability coefficient increases. This has important guiding significance for predicting the performance of FOPC and designing mix proportions.

(4) The dispersion of FOPC compressive strength under different aggregate sizes is similar, and its nominal strength roughly followed a normal distribution with a mean of 1 and a COV in the range of 0.10–0.15. The overall COV of the compressive strength of FOPC was approximately 0.132, and this is similar to the COV of ordinary concrete.

(5) The dispersion of the FOPC permeability coefficient under different aggregate sizes is similar; however, its distribution form was not like a normal distribution, and the COV ranged from 0.14 to 0.20, and with a COV of 0.15 for all samples.

(6) The statistical results of this study were obtained based on strict experimental conditions. In the preparation of pervious concrete for actual engineering pavement, due to the inability to guarantee preparation conditions, the discreteness of FOPC performance may be greater. The discreteness of actual FOPC performance is also something that needs to be considered in future research work.

(7) Employing original mix-ratio parameters in conjunction with machine learning methods accurately predicts concrete's compressive strength. An enhanced predictive model that incorporates both the original mix-ratio and porosity parameters shows high precision in forecasting the permeability coefficient, with Support Vector Machines (SVMs) achieving the highest accuracy.

Author Contributions: Conceptualization, Z.T., H.P. and F.F.; methodology, H.P., S.Y. and F.F.; validation, S.Y. and F.F.; formal analysis, S.Y.; investigation, F.F.; data curation, S.Y.; writing—original draft preparation, Z.T.; visualization, H.P. and F.F.; project administration, Z.T.; funding acquisition, Z.T. and H.P. All authors have read and agreed to the published version of the manuscript.

Funding: This research was funded by the “Social Welfare Research Fund of Ningbo Science and Technology Bureau in 2022”, grant number 2022S178 and the “Open Fund of National Engineering Laboratory for Applied Technology of Forestry & Ecology in South China in 2022”, grant number 2022NFLY01.

Data Availability Statement: Data is contained within the article.

Conflicts of Interest: The authors declare no conflicts of interest.

References

1. Huang, K.-L.; Song, Y.; Sheng, Y.-M. Rainstorm Resistance of Recycled Pervious Concrete under the Coupling of Fatigue and Freeze–Thaw Cycles. *Buildings* **2024**, *14*, 294. [[CrossRef](#)]
2. Lee, M.-G.; Wang, W.-C.; Wang, Y.-C.; Hsieh, Y.-C.; Lin, Y.-C. Mechanical Properties of High-Strength Pervious Concrete with Steel Fiber or Glass Fiber. *Buildings* **2022**, *12*, 620. [[CrossRef](#)]
3. Lee, M.-G.; Wang, Y.-C.; Wang, W.-C.; Chien, H.-J.; Cheng, L.-C. Experimental Study on the Mechanical Properties of Reinforced Pervious Concrete. *Buildings* **2023**, *13*, 2880. [[CrossRef](#)]
4. Lee, M.-G.; Wang, Y.-C.; Wang, W.-C.; Hsieh, Y.-C. Abrasion and Maintenance of High-Strength Fiber-Reinforced Pervious Concrete. *Buildings* **2024**, *14*, 127. [[CrossRef](#)]
5. Gao, S.; Huang, K.; Chu, W.; Wang, W. Feasibility Study of Pervious Concrete with Ceramsite as Aggregate Considering Mechanical Properties, Permeability, and Durability. *Materials* **2023**, *16*, 5127. [[CrossRef](#)] [[PubMed](#)]
6. Ferić, K.; Sathish Kumar, V.; Romić, A.; Gotovac, H. Effect of Aggregate Size and Compaction on the Strength and Hydraulic Properties of Pervious Concrete. *Sustainability* **2023**, *15*, 1146. [[CrossRef](#)]
7. Adil, G.; Kevern, J.T.; Mann, D. Influence of Silica Fume on Mechanical and Durability of Pervious Concrete. *Constr. Build. Mater.* **2020**, *247*, 118453. [[CrossRef](#)]

8. AlShareedah, O.; Nassiri, S. Pervious Concrete Mixture Optimization, Physical, and Mechanical Properties and Pavement Design: A Review. *J. Clean. Prod.* **2021**, *288*, 125095. [[CrossRef](#)]
9. Xie, X.; Zhang, T.; Wang, C.; Yang, Y.; Bogush, A.; Khayrulina, E.; Huang, Z.; Wei, J.; Yu, Q. Mixture Proportion Design of Pervious Concrete Based on the Relationships between Fundamental Properties and Skeleton Structures. *Cem. Concr. Compos.* **2020**, *113*, 103693. [[CrossRef](#)]
10. Xie, T.; Visintin, P.; Zhao, X.; Gravina, R. Mix Design and Mechanical Properties of Geopolymer and Alkali Activated Concrete: Review of the State-of-the-Art and the Development of a New Unified Approach. *Constr. Build. Mater.* **2020**, *256*, 119380. [[CrossRef](#)]
11. Wang, Z.; Zou, D.; Liu, T.; Zhou, A.; Shen, M. A Novel Method to Predict the Mesostructure and Performance of Pervious Concrete. *Constr. Build. Mater.* **2020**, *263*, 120117. [[CrossRef](#)]
12. Yan, X.; Wang, X.; Sun, C.; Xin, M.; He, J. Performance Analysis and Admixture Optimization of GBFS-HPMC/Fiber Pervious Concrete. *Materials* **2023**, *16*, 6455. [[CrossRef](#)] [[PubMed](#)]
13. Zhang, Q.; Feng, X.; Chen, X.; Lu, K. Mix Design for Recycled Aggregate Pervious Concrete Based on Response Surface Methodology. *Constr. Build. Mater.* **2020**, *259*, 119776. [[CrossRef](#)]
14. Han, S.H.; Khayat, K.H.; Park, S.; Yoon, J. Machine Learning-Based Approach for Optimizing Mixture Proportion of Recycled Plastic Aggregate Concrete Considering Compressive Strength, Dry Density, and Production Cost. *J. Build. Eng.* **2024**, *83*, 108393. [[CrossRef](#)]
15. Zhang, J.; Huang, Y.; Ma, G.; Sun, J.; Nener, B. A Metaheuristic-Optimized Multi-Output Model for Predicting Multiple Properties of Pervious Concrete. *Constr. Build. Mater.* **2020**, *249*, 118803. [[CrossRef](#)]
16. Sun, J.; Zhang, J.; Gu, Y.; Huang, Y.; Sun, Y.; Ma, G. Prediction of Permeability and Unconfined Compressive Strength of Pervious Concrete Using Evolved Support Vector Regression. *Constr. Build. Mater.* **2019**, *207*, 440–449. [[CrossRef](#)]
17. Jayasuriya, A.; Shibata, E.S.; Chen, T.; Adams, M.P. Development and Statistical Database Analysis of Hardened Concrete Properties Made with Recycled Concrete Aggregates. *Resour. Conserv. Recycl.* **2021**, *164*, 105121. [[CrossRef](#)]
18. Hou, D.; Li, D.; Hua, P.; Jiang, J.; Zhang, G. Statistical Modelling of Compressive Strength Controlled by Porosity and Pore Size Distribution for Cementitious Materials. *Cem. Concr. Compos.* **2019**, *96*, 11–20. [[CrossRef](#)]
19. Ding, X.; Zhao, M.; Zhou, S.; Fu, Y.; Li, C. Statistical Analysis and Preliminary Study on the Mix Proportion Design of Self-Compacting Steel Fiber Reinforced Concrete. *Materials* **2019**, *12*, 637. [[CrossRef](#)] [[PubMed](#)]
20. Sonebi, M.; Bassuoni, M.T. Investigating the Effect of Mixture Design Parameters on Pervious Concrete by Statistical Modelling. *Constr. Build. Mater.* **2013**, *38*, 147–154. [[CrossRef](#)]
21. Xie, H.-Z.; Li, L.G.; Ng, P.-L.; Liu, F. Effects of Solid Waste Reutilization on Performance of Pervious Concrete: A Review. *Sustainability* **2023**, *15*, 6105. [[CrossRef](#)]
22. Tamimi, A.; Tabsh, S.W.; El-Emam, M. Pervious Concrete Made with Recycled Coarse Aggregate and Reinforced with Date Palm Leaves Fibers. *Materials* **2023**, *16*, 7496. [[CrossRef](#)] [[PubMed](#)]
23. Mehrabi, P.; Shariati, M.; Kabirifar, K.; Jarrah, M.; Rasekh, H.; Trung, N.T.; Shariati, A.; Jahandari, S. Effect of Pumice Powder and Nano-Clay on the Strength and Permeability of Fiber-Reinforced Pervious Concrete Incorporating Recycled Concrete Aggregate. *Constr. Build. Mater.* **2021**, *287*, 122652. [[CrossRef](#)]
24. Liu, T.; Wang, Z.; Zou, D.; Zhou, A.; Du, J. Strength Enhancement of Recycled Aggregate Pervious Concrete Using a Cement Paste Redistribution Method. *Cem. Concr. Res.* **2019**, *122*, 72–82. [[CrossRef](#)]
25. Park, J.-H.; Jeong, S.-T.; Bui, Q.-T.; Yang, I.-H. Strength and Permeability Properties of Pervious Concrete Containing Coal Bottom Ash Aggregates. *Materials* **2022**, *15*, 7847. [[CrossRef](#)] [[PubMed](#)]
26. Lo, F.-C.; Lee, M.-G.; Lo, S.-L. Effect of Coal Ash and Rice Husk Ash Partial Replacement in Ordinary Portland Cement on Pervious Concrete. *Constr. Build. Mater.* **2021**, *286*, 122947. [[CrossRef](#)]
27. Shen, P.; Zheng, H.; Liu, S.; Lu, J.-X.; Poon, C.S. Development of High-Strength Pervious Concrete Incorporated with High Percentages of Waste Glass. *Cem. Concr. Compos.* **2020**, *114*, 103790. [[CrossRef](#)]
28. Saboo, N.; Shivhare, S.; Kori, K.K.; Chandrappa, A.K. Effect of Fly Ash and Metakaolin on Pervious Concrete Properties. *Constr. Build. Mater.* **2019**, *223*, 322–328. [[CrossRef](#)]
29. Chen, X.; Wang, H.; Najm, H.; Venkiteela, G.; Hencken, J. Evaluating Engineering Properties and Environmental Impact of Pervious Concrete with Fly Ash and Slag. *J. Clean. Prod.* **2019**, *237*, 117714. [[CrossRef](#)]
30. Bao, J.; Yu, Z.; Wang, L.; Zhang, P.; Wan, X.; Gao, S.; Zhao, T. Application of Ferronickel Slag as Fine Aggregate in Recycled Aggregate Concrete and the Effects on Transport Properties. *J. Clean. Prod.* **2021**, *304*, 127149. [[CrossRef](#)]
31. Qi, A.; Liu, X.; Wang, Z.; Chen, Z. Mechanical Properties of the Concrete Containing Ferronickel Slag and Blast Furnace Slag Powder. *Constr. Build. Mater.* **2020**, *231*, 117120. [[CrossRef](#)]
32. You, N.; Li, B.; Cao, R.; Shi, J.; Chen, C.; Zhang, Y. The Influence of Steel Slag and Ferronickel Slag on the Properties of Alkali-Activated Slag Mortar. *Constr. Build. Mater.* **2019**, *227*, 116614. [[CrossRef](#)]
33. Kim, H.; Lee, C.H.; Ann, K.Y. Feasibility of Ferronickel Slag Powder for Cementitious Binder in Concrete Mix. *Constr. Build. Mater.* **2019**, *207*, 693–705. [[CrossRef](#)]
34. Saha, A.K.; Sarker, P.K. Durability Characteristics of Concrete Using Ferronickel Slag Fine Aggregate and Fly Ash. *Mag. Concr. Res.* **2018**, *70*, 865–874. [[CrossRef](#)]

35. Chockalingam, T.; Vijayaprabha, C.; Leon Raj, J. Experimental Study on Size of Aggregates, Size and Shape of Specimens on Strength Characteristics of Pervious Concrete. *Constr. Build. Mater.* **2023**, *385*, 131320. [[CrossRef](#)]
36. Furkan Ozel, B.; Sakalli, S.; Şahin, Y. The Effects of Aggregate and Fiber Characteristics on the Properties of Pervious Concrete. *Constr. Build. Mater.* **2022**, *356*, 129294. [[CrossRef](#)]
37. Long, X.; Mao, M.; Su, T.; Su, Y.; Tian, M. Machine Learning Method to Predict Dynamic Compressive Response of Concrete-like Material at High Strain Rates. *Def. Technol.* **2023**, *23*, 100–111. [[CrossRef](#)]
38. He, H.; Shuang, E.; Ai, L.; Wang, X.; Yao, J.; He, C.; Cheng, B. Exploiting Machine Learning for Controlled Synthesis of Carbon Dots-Based Corrosion Inhibitors. *J. Clean. Prod.* **2023**, *419*, 138210. [[CrossRef](#)]
39. Li, D.; Nie, J.-H.; Wang, H.; Ren, W.-X. Loading Condition Monitoring of High-Strength Bolt Connections Based on Physics-Guided Deep Learning of Acoustic Emission Data. *Mech. Syst. Signal Process.* **2024**, *206*, 110908. [[CrossRef](#)]
40. GB/T50081-2016; Standard Test Methods for Mechanical Properties on Ordinary Concrete. Ministry of Housing and Urban-Rural Development: Beijing, China, 2019. (In Chinese)
41. CJJ/T135-2009; Technical Specification for Pervious Cement Concrete Pavement. Ministry of Housing and Urban-Rural Development: Beijing, China, 2009. (In Chinese)
42. Zheng, X.; Pan, J.; Easa, S.; Fu, T.; Liu, H.; Liu, W.; Qiu, R. Utilization of Copper Slag Waste in Alkali-Activated Metakaolin Pervious Concrete. *J. Build. Eng.* **2023**, *76*, 107246. [[CrossRef](#)]
43. Huang, D.-Q.; Li, P.-D. Effect of Aggregate Sizes on Dilation Properties and Stress—Strain Behavior of FRP-Confined Recycled Aggregate Concrete. *J. Build. Eng.* **2024**, *89*, 109245. [[CrossRef](#)]
44. Li, H.; Yang, J.; Yu, X.; Zhang, Y.; Zhang, L. Permeability Prediction of Pervious Concrete Based on Mix Proportions and Pore Characteristics. *Constr. Build. Mater.* **2023**, *395*, 132247. [[CrossRef](#)]
45. Liao, L.; Wu, S.; Hao, R.; Zhou, Y.; Xie, P. The Compressive Strength and Damage Mechanisms of Pervious Concrete Based on 2D Mesoscale Pore Characteristics. *Constr. Build. Mater.* **2023**, *386*, 131561. [[CrossRef](#)]
46. Strieder, H.L.; Dutra, V.F.P.; Graeff, Á.G.; Núñez, W.P.; Merten, F.R.M. Performance Evaluation of Pervious Concrete Pavements with Recycled Concrete Aggregate. *Constr. Build. Mater.* **2022**, *315*, 125384. [[CrossRef](#)]
47. Zhang, F.; Feng, F.; Liu, X. Reliability Analysis of Concrete Beam with High-Strength Steel Reinforcement. *Materials* **2022**, *15*, 8999. [[CrossRef](#)] [[PubMed](#)]
48. Rajakarunakaran, S.A.; Lourdu, A.R.; Muthusamy, S.; Panchal, H.; Jawad Alrubaie, A.; Musa Jaber, M.; Ali, M.H.; Tlili, I.; Maseleno, A.; Majdi, A.; et al. Prediction of Strength and Analysis in Self-Compacting Concrete Using Machine Learning Based Regression Techniques. *Adv. Eng. Softw.* **2022**, *173*, 103267. [[CrossRef](#)]
49. Ren, Q.; Ding, L.; Dai, X.; Jiang, Z.; De Schutter, G. Prediction of Compressive Strength of Concrete with Manufactured Sand by Ensemble Classification and Regression Tree Method. *J. Mater. Civ. Eng.* **2021**, *33*, 04021135. [[CrossRef](#)]
50. Abd, A.M.; Abd, S.M. Modelling the Strength of Lightweight Foamed Concrete Using Support Vector Machine (SVM). *Case Stud. Constr. Mater.* **2017**, *6*, 8–15. [[CrossRef](#)]
51. Woo, B.-H.; Ryou, J.-S.; Kim, J.Y.; Lee, B.; Gi Kim, H.; Kim, J.-S. Freeze-Thaw Durability Estimation for Concrete through the Gaussian Process Regression with Kernel Convolution. *Constr. Build. Mater.* **2023**, *400*, 132825. [[CrossRef](#)]

Disclaimer/Publisher’s Note: The statements, opinions and data contained in all publications are solely those of the individual author(s) and contributor(s) and not of MDPI and/or the editor(s). MDPI and/or the editor(s) disclaim responsibility for any injury to people or property resulting from any ideas, methods, instructions or products referred to in the content.